Correspondence

Exploiting Doppler in Bernoulli Track-Before-Detect for a Scanning Maritime Radar

Detection and tracking of small targets in sea clutter using high-resolution radar is a challenging problem. Recently, a Bernoulli track-before-detect (TBD) filter has been developed for an airborne scanning radar in the maritime domain, with the purpose of detection and tracking of short-exposure targets by using a fast scanning mode (i.e., short dwell-time and noncoherent integration). This article investigates the potential benefits of coherent radar processing and exploitation of Doppler information in TBD, when the radar operates in a slower scanning mode (i.e., using longer dwell times). For this purpose, a new Bernoulli TBD filter is developed, which is capable of processing full three-dimensional (range-azimuth-Doppler) radar data. The amplitude of sea clutter is modeled using the K distribution with Doppler-dependent shape and scale parameters. Numerical results indicate that the new Bernoulli TBD outperforms the fast scanning TBD filter, at signal-to-interference ratios below 6 dB.

I. INTRODUCTION

The conventional approach to target tracking, also referred to as detect-then-track, is based on point measurements obtained as outputs of a radar detection scheme. Choosing the detection threshold is very important as it determines the probability of target detection and the false alarm rate, thereby affecting the data flow and the complexity of the tracking operation. If the task is to detect and track targets characterized by a low signal-to-interference ratio (SIR), the threshold needs to be reduced in order to increase the probability of detection. However, this also increases the false alarm rate and, as a consequence, more sophisticated data association algorithms for tracking are required [1]. Furthermore, one can argue that by thresholding the radar data, one potentially throws away useful information and targets may be missed that are persistent with low SIRs.

Track-before-detect (TBD) is an alternative approach to detecting and tracking targets characterized by a low SIR: instead of point measurements, it uses the entire frame from a surveillance radar (e.g., a range-azimuth map) as a measurement. By removing the detection threshold, TBD

Manuscript received December 15, 2020; revised May 24, 2021 and June 19, 2021; released for publication June 20, 2021. Date of publication July 20, 2021; date of current version February 10, 2022.

DOI. No. 10.1109/TAES.2021.3098117

Refereeing of this contribution was handled by S. Maskell.

This work was supported by DST Group under the research agreement "Track-Before-Detect for Maritime Radar".

Authors' addresses: Branko Ristic, Du Yong Kim and Robin Guan are with the School of Engineering, RMIT University, Melbourne, VIC 3000, Australia, E-mail: (Branko.ristic@rmit.edu.au; duyong.kim@rmit.edu.au; robinping.guan@rmit.edu.au); Luke Rosenberg is with Defence Science and Technology Group, Edinburgh, SA 5111, Australia, E-mail: (Luke.Rosenberg@dst.defence.gov.au). *(Corresponding author: Branko Ristic.)*

makes full use of the radar data and enables lower SIR targets to be detected and reliably tracked [1]. The main idea of TBD is to exploit the persistence of targets over multiple consecutive scans, in combination with the motion model and the radar measurement model.

Early studies on TBD mainly focused on detection of small moving objects using imaging sensors (optical, infrared, noncoherent radar images) [2]–[4]. Pioneering works on TBD in the context of radar were reported in [5]–[7]. The TBD approach has since become widespread in the radar literature, resulting in a plethora of publications, e.g. [8]–[11]. Radar data differs from the imaging sensor data in several respects. First, it involves complex valued (range-azimuth) frames. Second, the interference consists of a superposition of clutter (returns from sea surface or ground) and thermal noise. Finally, due to the finite width of the antenna beam, a target is usually hit by several successive illuminations during each scan. Hence, in a radar context, targets are characterized not only by persistence over the successive scans, but also within each scan. This property can be exploited in the radar context to coherently integrate the back-scattered energy from the target during the dwell time.

The vast majority of TBD algorithms used in radar systems are solved using dynamic programming (or Viterbi) based algorithms. Despite its popularity, dynamic programming is a fairly cumbersome framework for online implementation of TBD, mainly due to the impracticality of discretizing the state-space in realistic problems and its requirement for high-dimensional maximization. An alternative is the recursive Bayesian estimation framework, first proposed in [12] and solved using the particle filter (PF) [13, Ch. 11]. Subsequently, a TBD PF was proposed in the context of radar processing [14] and image processing [15]. The recursive Bayesian framework for TBD became popular because the optimal Bayesian TBD for a single target can be formulated analytically as the Bernoulli TBD filter [16], [17]. Extensions to multitarget recursive Bayesian TBD were numerous, particularly using the random finite set framework [18]–[21]. Finally, it is worthwhile mentioning that some authors refer to TBD, an approach where detect-then-track is applied with a low detection threshold (referred to as *censoring*) and using the amplitude information of point measurements [22]. A comparison between the conventional detect-then-track approach with amplitude information and the Bernoulli TBD, carried out in the maritime surveillance context, showed that the latter performs significantly better when targets are weak and clutter is spiky [23].

In this article, we focus on TBD in the context of an airborne scanning radar for maritime surveillance. Detection and tracking of small maritime targets is a challenging problem due to the dynamics of sea-clutter and its non-Gaussian amplitude statistics [24]. Particularly at higher range resolutions and low grazing angles, the sea-clutter amplitude distribution is characterized by longer tails and is correlated both in space and time. Recently, we have developed a Bernoulli TBD filter for maritime radar as the optimal recursive Bayesian solution [25]. This filter was developed to detect and track short exposure targets using a short dwell-time and noncoherent integration in the fast scanning radar mode. The filter inputs the consecutive range-azimuth amplitude maps, and uses the K-distribution as a model for the clutter amplitude. It features the spatial decorrelation of clutter, an online parameter estimation scheme for the K-distribution parameters and is formulated for target amplitude fluctuations following the Swerling type 1 model. The filter was implemented numerically using the sequential Monte–Carlo method. Originally formulated for a single target, it was subsequently extended to multitarget TBD in [26].

For a scanning radar, the Doppler information can be obtained by taking the fast Fourier transform (FFT) of a block of pulses centered on the current azimuth location. The objective of the current article is to investigate the potential benefits of coherent radar processing (and the exploitation of Doppler information) in TBD, when the radar operates in a slower scanning mode using a longer dwell. On the one hand, a longer dwell is expected to result in an improved estimation for low SIR targets due to the longer integration time and associated frequency selectivity of coherent processing. However, a longer dwell means a lower update rate, which can manifest as a delay in track initiation and a reduction in track accuracy. In contrast to the approach presented in this article, exploitation of Doppler information in conventional target tracking using point measurements has focused primarily on improved velocity estimation, data association, and faster track initiation [27].

The contributions of this article are twofold. First, a new Bernoulli TBD filter, capable of exploiting the Doppler information by processing the full 3-D (range-azimuth-Doppler) radar data frames, is developed. The sea clutter amplitude in the Doppler domain is again modeled using the K-distribution with different shape and scale parameters for each frequency bin. The second contribution is a comparative performance analysis of Bernoulli TBD algorithms developed for slow and fast scanning radars. The preliminary results of this study were reported in [28].

The rest of the article is organized as follows. Section II reviews the radar data to be used in the study. Section III formulates the proposed TBD algorithm which exploits the Doppler information. A comparative performance study, quantifying the benefits of the slower scanning mode and Doppler information, is given in Section IV. Finally, Section V concludes this article.

II. RADAR DATA

A. Overview

In this study, the radar data was generated using the high-fidelity simulation environment for airborne maritime surveillance, described in [29]. The clutter component is K-distributed and correlated along both slow-time (pulses within the scan) and range, with the Doppler spectrum evolving in range.

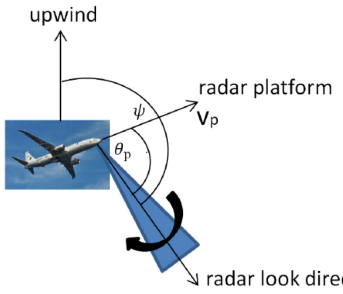

Fig. 1. Scanning airborne radar scenario [29].

TABLE I
Parameters of the Scanning Radar (See [29])

Parameter	value
Platform speed ($\lvert\mathbf{v}_\mathrm{p}\rvert$)	100 m/s
Platform heading ($\angle\mathbf{v}_\mathrm{p}$)	0° (North direction)
Wind & swell direction (ψ)	270°
Azimuth look direction (θ_p)	90°
Grazing angle	30°
Slant range offset to sea (km)	20
Sea state	3
Radar scan rate (ω_0)	
Slow scanning	20 rpm = $2\pi/3$ [rad/s]
Fast scanning	100 rpm = $10\pi/3$ [rad/s]
Azimuth 3 dB beamwidth ($\phi_{3\mathrm{dB}}$)	3°
Radar carrier frequency (f_0)	10 GHz
Bandwidth (B)	100 MHz
Pulse Repetition Frequency (f_r)	1500 Hz
Number of range bins (N_r)	500
Scanning region	30°

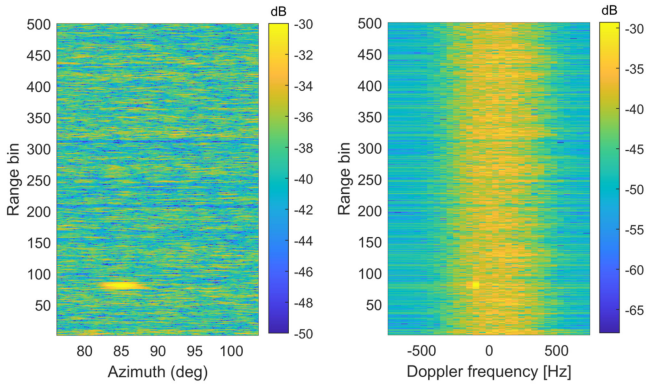

Fig. 2. Illustration of radar data obtained in the *slow* scanning mode. An SIR = 4 dB target is in range bin 80 with azimuth 85° and a Doppler frequency of −150 Hz. (a) Range-azimuth image (modulus) at Doppler bin corresponding to the frequency of −150 Hz. (b) Range-Doppler image centered at the azimuth bin corresponding to 85°.

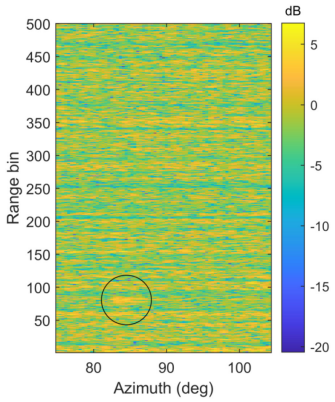

Fig. 3. Illustration of radar data obtained in the *fast* scanning mode: range-azimuth image. An SIR = 4 dB target is in range bin 80 with an azimuth of 85° (indicated by a circle).

Consider an airborne platform traveling with velocity $\mathbf{v}_\mathrm{p}$ and a scanning radar pointing at an angle θ_p relative to the platform motion [29], as illustrated in Fig. 1. The angle between the radar look direction and the wind is denoted by ψ. As the radar scans with a rate ω_0 (rad/s), there are $N_\mathrm{p} = 2\pi\ f_\mathrm{r}/\omega_0$ pulses in a given scan, where f_r is the pulse repetition frequency (PRF) of the radar. Also, if the two-way azimuth 3 dB beamwidth is $\phi_{3\mathrm{dB}}$, then a point target will be in the beam for $T_\tau = \phi_{3\mathrm{dB}}/\omega_0$ s or $N_\tau = \mathrm{floor}(T_\tau \cdot f_\mathrm{r})$ pulses. This limit determines the number of pulses which offer a coherent gain and can be exploited in the TBD algorithm.

First, we consider a slow scanning mode with $\omega_0 =$ 20 r/min, $f_\mathrm{r} = 1500$ Hz, and other simulation parameters givenin Table 1. The radar data from a single scan comprises slow-time and range, with the slow time dimension representing the radar return from different azimuth locations. To include Doppler, a sliding window of W pulses is Fourier-transformed and used to construct a three-dimensional complex-valued "frame" with dimensions of range, azimuth, and Doppler frequency. The radar revisits each azimuth look direction periodically, and hence the fourth dimension is the scan number. With this set of parameters, the radar scan time (an interval of time between two successive scans) is 3 s, with $N_\mathrm{p} = 4500$ pulses. Fig. 2(a) shows a side-looking region of data in the upwind direction, centered at the azimuth look direction of 90° and spread over the scanning region of 30°. In this scene, an outbound target is present with an SIR of 4 dB, moving with a radial velocity of 2.2 m/s (corresponding to a Doppler frequency of −150 Hz) and is located at 85° azimuth and range bin 80. The range-azimuth image in Fig. 2(a) represents the modulus of radar data in the range-azimuth subspace, taken in the Doppler cell containing the target Doppler of −150 Hz. The target appears spread along the azimuth direction, because it is illuminated by $N_\tau = 37$ pulses. The coherent processing exploits this effect by coherently integrating with a window of $W = 32$ pulses. Fig. 2(b) illustrates the range-Doppler image (modulus of radar data) with the FFT window centered at the azimuth bin corresponding to 85°.

Next we consider the same setup as above (the same target, radar parameters given in Table 1), except that the radar is now operating in the fast scanning mode, with 5 times higher scan rate of $\omega_0 = 100$ r/min. This corresponds to the radar scan time of 0.6 s and $N_\tau = 7$ pulses on target. Due to the short dwell time, only range-azimuth radar data are used in the Bernoulli TBD, as in [25]. Fig. 3 shows a side-looking region of the same scene. Comparing Fig. 3 with Fig. 2, we can observe that, even visually, the target is much

more pronounced when using a slow scanning mode. In addition, the slow scanning mode provides a measurement of the range-rate (via Doppler). The fast scanning mode, on the other hand, results in 5 times higher measurement update rate.

B. Clutter Modeling

Following [24], [30]–[32], the clutter amplitude, z, in each cell of radar data is modeled using the K-distribution

$$K(z;\nu_0,b)=\frac{4z^{\nu_0}}{\sqrt{b}^{\nu_0+1}\Gamma(\nu_0)}\kappa_{\nu_0-1}\left(\frac{2z}{\sqrt{b}}\right) \tag{1}$$

where ν_0 and b are the shape and scale parameters, respectively; and $\Gamma(\cdot)$ denotes the gamma function and $\kappa_n(\cdot)$ refers to the modified Bessel function of the second kind. To include additive thermal noise in the amplitude distribution [33], we define an "effective" shape parameter ν, which substitutes the shape parameter ν_0. This can be achieved by matching the moments of the probability density function (PDF) with and without noise [24], giving $\nu=\nu_0(1+1/C)^2$, where C is the clutter-to-noise ratio (CNR). For the remainder of the article, we will use ν as the shape parameter of *interference* (meaning, clutter plus thermal noise), without explicitly defining the CNR.

The K distribution is a widespread model for representing non-Gaussian sea clutter. For smaller values of ν, its distribution tail is longer, while for $\nu\to\infty$, it is approaching the Rayleigh distribution [24]. The K distribution has finite moments; its mean is given by [24, Ch. 6]

$$\mu=\sqrt{b}\frac{\Gamma(1.5)\,\Gamma(\nu+0.5)}{\Gamma(\nu)}. \tag{2}$$

The parameters of the K distribution (the shape ν and scale b) are homogeneous across the range and azimuth; however, they vary with the Doppler frequency [24], [30], [31]. Fig. 4 displays the shape and scale, estimated from five scans of radar data (in the absence of a target and using the slow scanning mode, with parameters given in Table 1), as a function of Doppler frequency. The shape parameter is characterized by lower values where the clutter is dominant (-200 to 400 Hz) with a peak around -300 Hz, where thermal noise has the greatest contribution. In this example, there is aliasing present due to the choice of PRF and the broad Doppler spectrum, which reduces the shape parameter outside of the clutter region. Parameter estimation was carried out using the moment based method [34]. Given L samples of amplitude values in Doppler cell $d=1,\ldots,W$, i.e., $\{z_1^d,\ldots,z_L^d\}$, the shape parameter is estimated as

$$\widehat{\nu}_d=\frac{1}{4}\left[\ln\left(\frac{\pi\,\widehat{m}_2^d}{4\,(\widehat{m}_1^d)^2}\right)\right]^{-1} \tag{3}$$

where

$$\widehat{m}_1^d=\frac{1}{L}\sum_{l=1}^{L}z_l^d,\qquad \widehat{m}_2^d=\frac{1}{L}\sum_{l=1}^{L}(z_l^d)^2 \tag{4}$$

are the first and second sample moments. The scale estimates are obtained as $\widehat{b}_d=\widehat{m}_2^d/\widehat{\nu}_d$. Fig. 4 also displays the resulting estimate of the interference mean, as a function of Doppler frequency, computed using (2). Note that the model parameters are representing an underlying swell in the scene, and hence the interference mean is slightly shifted toward the positive Doppler frequency.

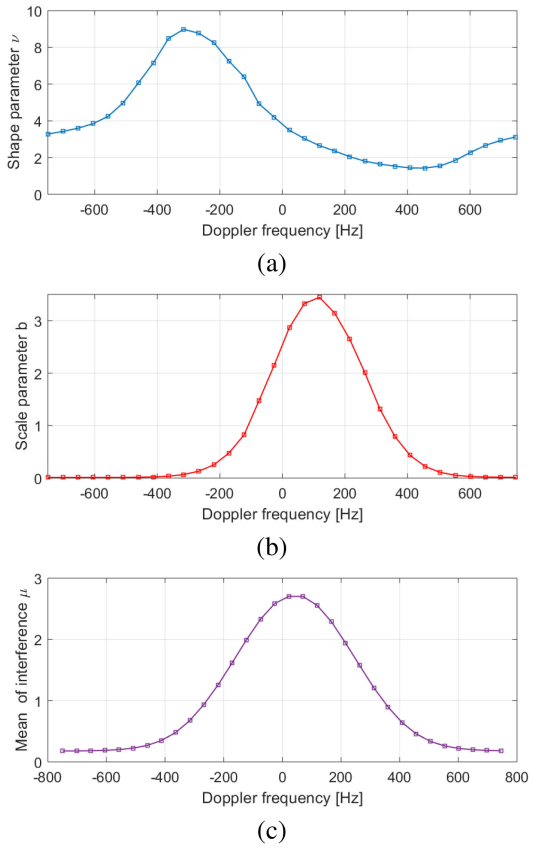

Fig. 4. Estimated values of (a) shape $\widehat{\nu}$ and (b) scale $\widehat{b}$ and (c) the mean of the interference as a function of Doppler frequency. Parameter estimation was carried out using the moment based method from five scans of radar data in the absence of a target and using the slow scanning mode, with parameters given in Table 1.

III. BERNOULLI TBD FOR MARITIME RANGE-AZIMUTH-DOPPLER DATA

A. Modeling

The models to be used for Bernoulli TBD filter are similar to those adopted in [25]. Because the observed region on the sea-surface is far from the airborne platform, we approximate the observed arc-shaped region of the sea surface with a rectangular region, and adopt the target state vector in Cartesian coordinates.[1] Thus, the state of the target at scan k is defined as $\mathbf{x}_k=[x_k\ \ \dot{x}_k\ \ y_k\ \ \dot{y}_k\ \ \chi_k]^\intercal$, where x_k, $\dot{x}_k$, y_k, and $\dot{y}_k$ are its azimuth, azimuth-rate, range, and range-rate, respectively. The fifth component, χ_k, is the mean intensity of the target signal. The units of x_k and y_k are adopted as the number of cells.

[1]Cartesian coordinates are an approximation, which can be justified in a typical airborne surveillance scenario, because the slant range is large (according to Table 1, 20 km).

The model of target state evolution is adopted as the nearly constant velocity motion model [35] with the transition density given by

$$\varphi_{k|k-1}(\mathbf{x}_k|\mathbf{x}_{k-1}) = \mathcal{N}(\mathbf{x}_k; \mathbf{F}\mathbf{x}_{k-1}, \mathbf{Q}) \tag{5}$$

where $\mathcal{N}(\mathbf{x}; \boldsymbol{\mu}, \boldsymbol{\Sigma})$ denotes the Gaussian PDF, evaluated at $\mathbf{x}$, with the mean $\boldsymbol{\mu}$ and covariance matrix $\boldsymbol{\Sigma}$. Matrices $\mathbf{F}$ and $\mathbf{Q}$ represent the transition matrix and the process noise covariance matrix, respectively. They are given by [35]

$$\mathbf{F} = \begin{bmatrix} \boldsymbol{\Phi} & 0 & 0 \\ 0 & \boldsymbol{\Phi} & 0 \\ 0 & 0 & 1 \end{bmatrix}, \qquad \boldsymbol{\Phi} = \begin{bmatrix} 1 & T \\ 0 & 1 \end{bmatrix} \tag{6}$$

$$\mathbf{Q} = \begin{bmatrix} \boldsymbol{\Psi} & 0 & 0 \\ 0 & \boldsymbol{\Psi} & 0 \\ 0 & 0 & q_{\mathrm{i}}T \end{bmatrix}, \qquad \boldsymbol{\Psi} = q_{\mathrm{s}} \begin{bmatrix} T^3/3 & T^2/2 \\ T^2/2 & T \end{bmatrix} \tag{7}$$

where T is the scan time; q_{s} and q_{i} denote the process noise intensity in the spatial and amplitude domains, respectively.

In order to detect a target in TBD, it is convenient to introduce a binary random variable $\epsilon_k \in \{0, 1\}$, such that, by convention, $\epsilon_k = 1$ means that the target is present and conversely $\epsilon_k = 0$ that the target is absent. The dynamics of ϵ_k are modeled by the first-order two-state Markov chain, whose transitional probability matrix is given by

$$\boldsymbol{\Pi} = \begin{bmatrix} 1 - p_{\mathrm{b}} & p_{\mathrm{b}} \\ 1 - p_{\mathrm{s}} & p_{\mathrm{s}} \end{bmatrix} \tag{8}$$

where $p_{\mathrm{b}} = P\{\epsilon_{k+1} = 1|\epsilon_k = 0\}$ and $p_{\mathrm{s}} = P\{\epsilon_{k+1} = 1|\epsilon_k = 1\}$ are referred to as the probability of *target birth* and *target survival*, respectively.[2] If the target appears at scan $k-1$, its state vector can be seen as a random sample from the birth density $b_{k-1|k-1}(\mathbf{x})$. Practical implementation of the birth density will be discussed in Section III-C.

The measurement used by the TBD algorithm at scan k is the modulus of the range-azimuth-Doppler data, denoted by $\mathbf{z}_k$. The PDF of a measured value z in the (m, n, d)th cell of $\mathbf{z}_k$, for $m = 1, \ldots, N_{\mathrm{r}}$, $n = 1, \ldots, N_{\mathrm{a}}$ and $d = 1, \ldots, W$, will be presented next for two cases: the interference only case and the target plus interference case.

We have already stated that the measured amplitude z in each cell of $\mathbf{z}_k$, if due to interference only, is modeled with the K-distribution, i.e.,

$$p_0^{(m,n,d)}(z) = K\left(z; \nu_d, b_d\right). \tag{9}$$

The contribution of a target in the state $\mathbf{x} = [x,\ \dot{x},\ y\ \dot{y},\ \chi]^{\intercal}$ to the measured value z in the (m, n, d)th cell is expressed via the point spread function (PSF). Let us adopt a Gaussian PSF

$$h^{(m,n,d)}(\mathbf{x}) = \frac{\chi}{\alpha} \exp\left[-\frac{(m-x)^2}{2\sigma_x^2} - \frac{(n-y)^2}{2\sigma_y^2} - \frac{(d-D)^2}{2\sigma_D^2} \right] \tag{10}$$

where χ is the target mean intensity, $\alpha = (2\pi)^{3/2}\sigma_x\sigma_y\sigma_D$, and $\sigma_x \ll N_{\mathrm{a}}$, $\sigma_y \ll N_{\mathrm{r}}$ and $\sigma_D \ll W$ determine the spread of the Gaussian PSF in azimuth, range, and Doppler measurement coordinates, respectively. Note that the Doppler frequency D in (10) is linearly related to the range-rate, that is, $D = -2\dot{y}f_0/B$, where f_0 is the carrier frequency and B is the radar bandwidth (see Table 1). The spread of the Gaussian PSF models the target amplitude contribution to its neighboring cells in azimuth, range, and Doppler. This spread is particularly large in azimuth, as we discussed in relation to Fig. 2.

The PDF of measured amplitude z in the (m, n, d)th cell of $\mathbf{z}_k$, for the case of a Swerling 1 target in K distributed interference, is referred to as the L-distribution [25], i.e.,

$$p_1^{(m,n,d)}(z|\mathbf{x}) = L\left(z; h^{(m,n,d)}(\mathbf{x}), \nu_d, b_d\right). \tag{11}$$

The L-distribution can only be expressed in an integral form as [25], [36]

$$L(z; h, \nu, b) = \frac{2z}{b^{\nu}\Gamma(\nu)} \int_0^{\infty} \frac{\eta^{\nu-1}}{\eta + h} \exp\left[-\frac{z^2}{\eta + h} - \frac{\eta}{b} \right] d\eta. \tag{12}$$

By setting $h = 0$ in (12), L-distribution reduces to the K-distribution.

B. TBD Algorithm

The Bernoulli TBD filter is the optimal Bayesian track-before-detect algorithm [16]. It propagates two quantities over time. The first is the posterior probability of target presence $q_{k|k} = P\{\epsilon_k = 1|\mathbf{z}_{1:k}\}$, where $\mathbf{z}_{1:k} \equiv \mathbf{z}_1, \ldots, \mathbf{z}_k$ is the sequence of radar measurements from scan 1 to scan k. The second quantity is the posterior spatial probability distribution $s_{k|k}(\mathbf{x}) = p_k(\mathbf{x}|\mathbf{z}_{1:k})$, conditioned on target presence. Assuming that at time $k-1$, both $q_{k-1|k-1}$ and $s_{k-1|k-1}(\cdot)$ are available, the Bernoulli TBD filter provides the recursive formulae for the computation of $q_{k|k}$ and $s_{k|k}(\cdot)$. This computation is carried out in two steps, the prediction and update.

Given the pair $(q_{k-1|k-1}, s_{k-1|k-1})$, the prediction equations of the Bernoulli filter are as follows [16]:

$$q_{k|k-1} = p_b\left(1 - q_{k-1|k-1}\right) + p_s\, q_{k-1|k-1} \tag{13}$$

$$s_{k|k-1}(\mathbf{x}) = \frac{p_b\left(1 - q_{k-1|k-1}\right) \int \varphi_{k|k-1}(\mathbf{x}|\mathbf{x}')\, b_{k-1|k-1}(\mathbf{x}')d\mathbf{x}'}{q_{k|k-1}} + \frac{p_s\, q_{k-1|k-1} \int \varphi_{k|k-1}(\mathbf{x}|\mathbf{x}')\, s_{k-1|k-1}(\mathbf{x}')d\mathbf{x}'}{q_{k|k-1}} \tag{14}$$

where $b_{k-1|k-1}(\mathbf{x})$, referred to as the target birth density, is the probability density over the state-space which models the state of the target if it has appeared at scan $k-1$. A practical design of $b_{k-1|k-1}(\mathbf{x})$ will be discussed in Section III-C.

The update equations of the Bernoulli TBD filter are given by

$$q_{k|k} = \frac{q_{k|k-1} \int \ell(\mathbf{z}_k|\mathbf{x})\, s_{k|k-1}(\mathbf{x})\, d\mathbf{x}}{1 - q_{k|k-1} + q_{k|k-1} \int \ell(\mathbf{z}_k|\mathbf{x})\, s_{k|k-1}(\mathbf{x})\, d\mathbf{x}} \tag{15}$$

[2] Probability p_{b} is typically a small number, because targets appear rarely in the surveillance volume; p_{s} is typically close to (but less than) 1, because a target, when it appears, tends to be present for many scans.

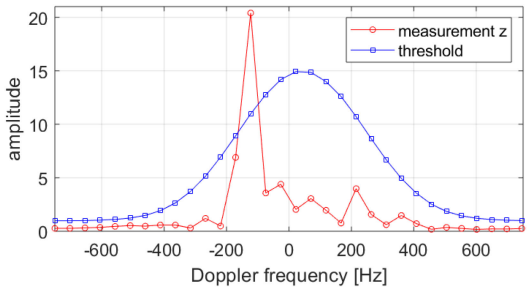

Fig. 5. Illustration of the birth density design: red line is the Doppler spectrum at range-azimuth cell in which the target is present; the blue line is the threshold $\hbar$.

$$s_{k|k}(\mathbf{x}) = \frac{\ell(\mathbf{z}_k|\mathbf{x})\, s_{k|k-1}(\mathbf{x})}{\int \ell(\mathbf{z}_k|\mathbf{x})\, s_{k|k-1}(\mathbf{x})\, d\mathbf{x}} \tag{16}$$

where $\ell(\mathbf{z}_k|\mathbf{x})$ is the likelihood ratio defined as

$$\ell(\mathbf{z}_k|\mathbf{x}) = \prod_{m=1}^{N_a}\prod_{n=1}^{N_r}\prod_{d=1}^{W} \frac{p_1^{(m,n,d)}(z|\mathbf{x})}{p_0^{(m,n,d)}(z)} \tag{17}$$

with likelihood functions $p_1^{(m,n,d)}(\cdot|\mathbf{x}_k)$ and $p_0^{(m,n,d)}(\cdot)$ introduced in (11) and (9), respectively.

The Bernoulli TBD filter reports a detection only if $q_{k|k} > \xi$, where ξ is a parameter referred to as the reporting threshold.

C. Implementation Notes

Because there is no analytic closed form solution to the Bernoulli TBD filter, it is implemented using the sequential Monte–Carlo method, as a PF [16], [25]. The spatial distribution $s_{k|k}(\cdot)$ is approximated by a random weighted sample $\{w_{k|k}^{(i)}, \mathbf{x}_{k|k}^{(i)}\}_{1\le i\le S}$, where $\mathbf{x}_{k|k}^{(i)}$ is the ith sample (particle), $w_{k|k}^{(i)}$ is its normalized weight, and S is the sample size. This approximation simplifies the computation of integrals in (14)–(16). The proposal distribution is adopted as the transitional density $\varphi_{k|k-1}$ given by (5). More detailed explanation can be found in [16].

The likelihood ratio (17) needs to be computed for every particle. First, the index triple (m_i, n_i, d_i), corresponding to the particle $\mathbf{x}_{k|k}^{(i)}$, $i = 1, \ldots, S$, is determined. Then, in order to speed up the computation of (17), each product is computed for a subset of indices in the vicinity of (m_i, n_i, d_i), that is, for $m = m_i - U_m, \ldots, m_i + U_m$, $n = n_i - U_n, \ldots, n_i + U_n$, and $d = d_i - U_D, \ldots, d_i + U_D$. The values of U_m, U_n, and U_D are adopted to correspond to the spread factors of the Gaussian PSF, i.e., σ_x, σ_y, and σ_D in (10), respectively.

The birth density $b_{k-1|k-1}$ is measurement driven [37]: it is approximated with a random weighted sample using $\mathbf{z}_{k-1}$ as follows. In the $(x, y, \dot{y})$ subspace, the samples are drawn to correspond to the cells of $\mathbf{z}_{k-1}$ whose amplitude is above a Doppler frequency-dependent threshold $\hbar_d = \beta\mu_d$, where $\beta > 1$, for all range-azimuth indices. In order to illustrate this, in Fig. 5, we show a slice of Fig. 2(b) at range cell 80 (red line); this is a Doppler spectrum at range-azimuth cell in which the 4-dB target is present. Importantly, Fig. 5 illustrates the threshold $\hbar_k$ (blue line), obtained by multiplying the mean μ_d, shown in Fig. 4(c), with the coefficient β set at 5.5. Parameter β is a tuning parameter, chosen as a trade-off between the computational load (corresponding to the number of birth particles, required to adequately approximate the birth density), and the capability to detect/track low SIR targets. In every cell (m, n, d) of $\mathbf{z}_k$, in which the measured amplitude $z^{(m,n,d)} > \hbar$, we draw L random samples in x, y, and $\dot{y}$ subspace of the state-space, corresponding to (m, n, d) and taking into account the resolution of the radar cell. In the subspace of $\dot{x}$ (i.e., the speed in the azimuth direction), a uniform distribution is adopted with an adequate interval (corresponding to the maximum expected speed of the target). Finally, in the subspace of the mean target intensity χ, the birth density is a gamma distribution with parameters $(\kappa_\chi, \theta_\chi)$, where κ_χ is proportional to the estimated mean $\mu(d)$ [see Fig. 4(c)], while θ_χ is chosen so that it covers the interval of SIR values of interest.

IV. PERFORMANCE ANALYSIS

A. Simulation Setup and Parameters

For the simulation, the radar parameters are the same as in Table 1, with $N_a = 375$. The target is outbound, moving from range bin 80 with a radial velocity of 2.2 m/s, but stays in the azimuth bin corresponding to 85°. The scenario lasts 90 s, with the scan time for the slow scanning mode, $\omega_0 = 20$ r/min (see Table 1), is $T = 60/\omega_0 = 3$ s, resulting in 30 radar measurements $\mathbf{z}_k$ available for processing during the observation period. The scan time for the fast scanning mode ($\omega_0 = 100$ r/min) is $T = 60/\omega_0 = 0.6$ s, and hence 150 measurements are available during the observation period.

Three TBD filters will be compared in the context of maritime radar. The first is the Bernoulli TBD filter presented in this article, developed for the slow scanning mode. It will be denoted Bern-TBD-Slow-3D. The second is the Bernoulli TBD filter presented in [28]: it is also developed for the slow scanning mode; however, it does not process the full three-dimensional radar data using the TBD approach. Instead, it extracts the Doppler information as a point measurement, and applies the TBD paradigm to the range-azimuth maps. This method will be referred to as Bern-TBD-Slow-2D. Finally, the third is the Bernoulli TBD filter developed for the fast scanning mode, described in [25]. We point out that in the fast scanning mode, the Doppler information is poor and hence is not used. This TBD filter will be denoted by Bern-TBD-Fast. The parameters used in all the three Bernoulli TBD filters were as follows: process noise parameters $q_s = 0.1$, $q_i = 1.5$; dynamic model parameters $p_b = 0.01$, $p_s = 0.99$; number of particles $S = 7500$; the Gaussian PSF parameters: $\sigma_x = 2$ for Bern-TBD-Fast and $\sigma_x = 6$ for Bern-TBD-Slow-3D and Bern-TBD-Slow-2D, $\sigma_y = 1.2$ (for all) and $\sigma_D = 0.7$ (for Bern-TBD-Slow-3D only). Accordingly, we adopted $U_m = 4$, $U_n = 1$, and $U_d = 1$. The birth density parameters κ_χ and θ_χ, as well as the reporting threshold ξ, were tuned so that

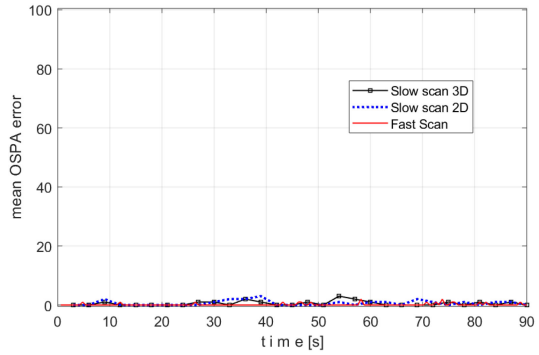

Fig. 6. Mean OSPA positional errors of Bernoulli TBD filters in the absence of a target.

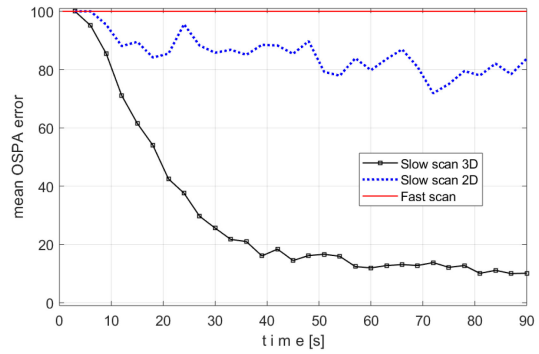

Fig. 7. Mean OSPA positional errors of Bernoulli TBD filters for a target at SIR = 0 dB.

all three Bernoulli TBD filters achieve a similar false track declaration rate. For the Bern-TBD-Slow-3D, parameter κ_χ depends on Doppler, and is adopted as $\kappa_\chi = 9\,\mu(d)$, with $\theta_\chi = 3$ and $\xi = 0.85$.

Joint detection and tracking performance is measured using the mean optimal subpattern assignment (OSPA) metric [38]. This metric penalizes both the error in the number of targets (zero or one in our case) and the error in the target position, but does not consider the target velocity and mean power in the performance assessment. The positional error is expressed in the units of cells. The OSPA metric has two parameters, order p and the cut-off c. In simulations, we set $p = 2$, so the metric is an ℓ_2 norm measure. The parameter c, which expresses the penalty assigned to the cardinality error in terms of the number of cells, is set to $c = 100$. The mean OSPA metric is estimated by averaging over 100 Monte–Carlo runs.

B. Results

The performance results for the three Bernoulli TBD filters are shown in Figs. 6– 10. Fig. 6 presents the mean OSPA error in the absence of a target, and its purpose is to establish the rate of false track declarations. One can observe from Fig. 6 that for all three Bernoulli TBD filters, the mean OSPA error is close to zero. The measured false track declaration rate for all three TBD filters is approximately equal to 0.002/s.

Figs. 7–10 display the mean OSPA error curves in the presence of a target, with SIRs equal to 0, 2, 4, and 6 dB. In all figures, the initial mean OSPA error equals $c = 100$,

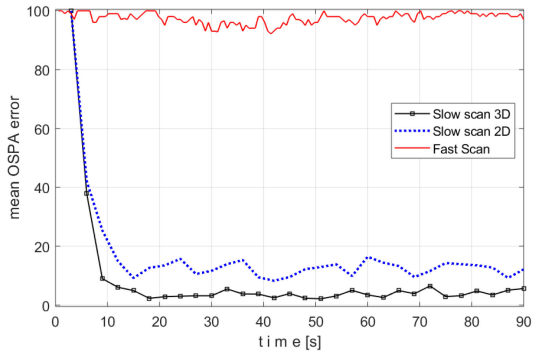

Fig. 8. Mean OSPA positional errors of Bernoulli TBD filters for a target at SIR = 2 dB.

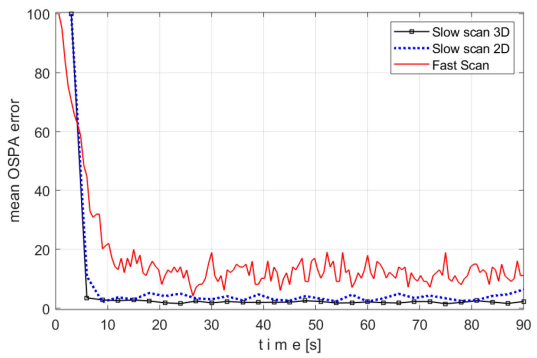

Fig. 9. Mean OSPA positional errors of Bernoulli TBD filters for a target at SIR = 4 dB.

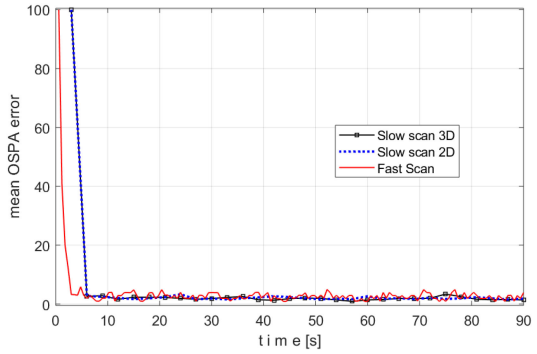

Fig. 10. Mean OSPA positional errors of Bernoulli TBD filters for a target at SIR = 6 dB.

because the Bernoulli TBD filter requires at least one scan of radar data to establish a track. For the case of a 0 dB target (Fig. 7), the Bern-TBD-Slow-3D is capable of establishing a track on the target with a delay of about 40 s. Once the track has been established, the OSPA error remains somewhat elevated (at the level of about 10–15), because the posterior probability of track presence $q_{k|k}$ occasionally falls below the reporting threshold ξ. Note that the other two Bernoulli TBD filters (Bern-TBD-Slow-2D and Bern-TBD-Fast) perform much worse: they are unable to reliably detect and track the target at SIR = 0 dB.

For the case of a target at SIR = 2 dB (Fig. 8), both Bernoulli TBD filters which exploit the Doppler information in the slow scanning mode (i.e. Bern-TBD-Slow-3D and Bern-TBD-Slow-2D), significantly outperform the Bern-TBD-Fast. The latter appears to be effectively blind

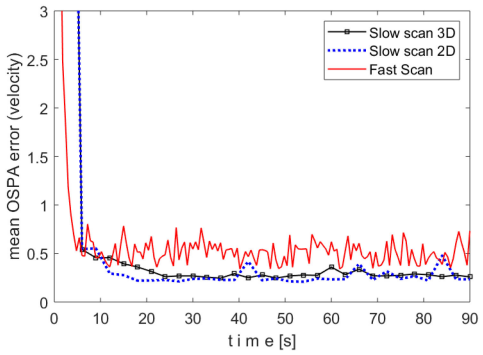

Fig. 11. Mean OSPA velocity errors of Bernoulli TBD filters for a target at SIR = 6 dB.

to the existence of a target for SIRs less than or equal to 2 dB, and consequently is unable to establish a track on it. The algorithm developed in this article, which exploits the full 3D radar data (Bern-TBD-Slow-3D), produces slightly better results than Bern-TBD-Slow-2D: it established a track on the target in less than 10 s and maintains it reliably throughout the observation period.

For the case of a target at SIR $\geq$ 4 dB (Figs. 9 and 10), the two Bernoulli TBD filters which exploit the Doppler information in the slow scanning mode (i.e. Bern-TBD-Slow-3D and Bern-TBD-Slow-2D) perform almost identically. They need 6 s to establish a track on the target and subsequently maintain the track with a minimal error. At SIR = 4 dB, even the performance of the Bern-TBD-Fast improves considerably (Fig. 9); because of the higher update rate (i.e., shorter scan time), the track is established almost as quickly as in the Bern-TBD-Slow, although the steady-state mean OSPA error remains about two to three times higher. For a target at SIR = 6 dB (or higher), the Bern-TBD-Fast performs better than the two Bernoulli TBD filters in the slow scanning mode: its steady-state error is the same, but due to the higher update rate, it establishes a track quicker (3 s instead of 6 s).

Finally, Fig. 11 displays the mean OSPA curves for velocity error in the presence of a target characterized with SIR = 6 dB. The OSPA parameters for velocity error are set to $c = 10$ and $p = 2$. We can observe from Fig. 11 that velocity errors are smaller for the two Bernoulli TBD filters that exploit Doppler information.[3]

In summary, we can observe that with more pulses on the target, the Doppler information becomes beneficial at low SIR values (below 6 dB): it improves both the detection and tracking performance of the TBD filter. The improved performance is due to coherent gain: in the slow scanning mode, the CPI of 32 pulses gives a gain of 15 dB, while for the fast scanning mode, there are only seven pulses that cover the target and the gain is reduced to 8.5 dB. The price for the increased number of pulses on target is either a slower scan rate (which is impractical for short-exposure targets), a higher PRF (which reduces the unambiguous range), or a wider beamwidth (an antenna constraint). For SIR values equal or greater than 6 dB, it appears that there is no advantage in using the Doppler information.

[3]Note, however, that the primary purpose of coherent radar processing and exploitation of Doppler in the slow scanning mode is not to improve the estimation error in velocity, but to detect and track targets at lower SIR.

V. CONCLUSION

This article explored the utilization of Doppler information in TBD for an airborne scanning maritime radar in a slow scanning mode. A new Bayesian-type Bernoulli TBD filter is developed, which exploits the full 3D radar data, including the Doppler spectrum. The filter is tuned to the Swerling 1 target in K distributed interference, because both models are commonly used to explain target fluctuations for a scanning maritime radar. The presented approach, however, is general in the sense that it is applicable to any other Swerling type or interference distribution by replacing (1) and (12) with the appropriate expressions for amplitude PDFs. The simulation results demonstrated that coherent radar processing using longer dwell-times in a slow scanning mode significantly improves the detection and tracking performance for persistent targets characterized by a low signal-to-interference ratio (either due to lower RCS or longer ranges). Future work will extend the proposed algorithm to the multitarget case.

BRANKO RISTIC
DU YONG KIM
School of Engineering, RMIT University
Melbourne, VIC 3000, Australia

LUKE ROSENBERG, *Senior Member, IEEE*
Defence Science, and Technology Group
Canberra, ACT, Australia

ROBIN GUAN
School of Engineering, RMIT University
Melbourne, VIC 3000, Australia

REFERENCES

[1] S. Blackman and R. Popoli
Design and Analysis of Modern Tracking Systems. Artech House, Boston, 1999.

[2] Y. Barniv
Dynamic programming solution for detecting dim moving targets
IEEE Trans. Aerosp. Electron. Syst., vol. 21, no. 1, pp. 144–156, Jan. 1985.

[3] I. S. Reed, R. M. Gagliardi, and L. B. Stotts
A recursive moving-target-indication algorithm for optical image sequences
IEEE Trans. Aerosp. Electron. Syst., vol. 26, no. 3, pp. 434–440, May 1990.

[4] B. Carlson, E. Evans, and S. Wilson
Search radar detection and track with the Hough transform. Part I: System concept
IEEE Trans. Aerosp. Electron. Syst., vol. 30, no. 1, pp. 102–108, Jan. 1994.

[5] W. R. Wallace
The use of track-before-detect in pulse-doppler radar
in *Proc. RADAR*, 2002, pp. 315–319.

[6] J. Kramer and W. Reid
Track-before-detect processing for an airborne type radar
in *Proc. IEEE Int. Conf. Radar*, 1990, pp. 422–427.

[7] S. Buzzi, M. Lops, and L. Venturino
Track-before-detect procedures for early detection of moving target from airborne radars
IEEE Trans. Aerosp. Electron. Syst., vol. 41, no. 3, pp. 937–954, Jul. 2005.

[8] X. Deng, Y. Pi, M. Morelande, and B. Moran
Track-before-detect procedures for low pulse repetition frequency surveillance radars
IET Radar Sonar Navigation, vol. 5, no. 1, pp. 65–73, 2011.

[9] H. Jiang, W. Yi, T. Kirubarajan, L. Kong, and X. Yang
Multiframe radar detection of fluctuating targets using phase information
IEEE Trans. Aerosp. Electron. Syst., vol. 53, no. 2, pp. 736–749, Apr. 2017.

[10] J. Gao, J. Du, and W. Wang
Radar detection of fluctuating targets under heavy-tailed clutter using track-before-detect
Sensors, vol. 18, no. 7, p. 2241, 2018.

[11] G. Zhou and L. Wang
Pseudo-spectrum based speed square filter for track-before-detect in range-doppler domain
IEEE Trans. Signal Process., vol. 67, no. 21, pp. 5596–5610, 2019.

[12] D. Salmond and H. Birch
A particle filter for track-before-detect
in *Proc. Am. Control Conf.*, 2001, pp. 3755–3760.

[13] B. Ristic, S. Arulampalam, and N. Gordon
Beyond the Kalman Filter: Particle Filters for Tracking Applications. Artech House, Boston, 2004.

[14] Y. Boers and J. Driessen
Multitarget particle filter track before detect application
IEE Proc. Radar Sonar Navigation, vol. 151, no. 6, pp. 351–357, 2004.

[15] M. G. S. Bruno
Bayesian methods for multiaspect target tracking in image sequences
IEEE Trans. Signal Process., vol. 52, no. 7, pp. 1848–1861, Jul. 2004.

[16] B. Ristic, B.-T. Vo, B.-N. Vo, and A. Farina
A tutorial on Bernoulli filters: Theory, implementation and applications
IEEE Trans. Signal Process., vol. 61, no. 13, pp. 3406–3430, Jul. 2013.

[17] F. Papi, V. Kyovtorov, R. Giuliani, F. Oliveri, and D. Tarchi
Bernoulli filter for track-before-detect using MIMO radar
IEEE Signal Process. Lett., vol. 21, no. 9, pp. 1145–1149, Sep. 2014.

[18] B.-N. Vo, B.-T. Vo, N.-T. Pham, and D. Suter
Joint detection and estimation of multiple objects from image observations
IEEE Trans. Signal Process., vol. 58, no. 10, pp. 5129–5141, Oct. 2010.

[19] F. Papi and D. Y. Kim
A particle multi-target tracker for superpositional measurements using labeled random finite sets
IEEE Trans. Signal Process., vol. 63, no. 16, pp. 4348–4358, Aug. 2015.

[20] D. Y. Kim
Multi-target track before detect with labeled random finite set and adaptive correlation filtering
in *Proc. Int. Conf. Control, Automat. Inf. Sci.*., 2017, pp. 44–49.

[21] A. F. Garcia-Fernandez
Track-before-detect labeled multi-Bernoulli particle filter with label switching
IEEE Trans. Aerosp. Electron. Syst., vol. 52, no. 5, pp. 2123–2138, Oct. 2016.

[22] E. Grossi, M. Lops, and L. Venturino
A track-before-detect algorithm with thresholded observations and closely-spaced targets
IEEE Signal Process. Lett., vol. 20, no. 12, pp. 1171–1174, Dec. 2013.

[23] B. Ristic, L. Rosenberg, D. Y. Kim, and R. Guan
Bernoulli filter for tracking maritime targets using point measurements with amplitude
Signal Process., vol. 181, 2021, Art. no. 107919.

[24] K. D. Ward, R. J. A. Tough, and S. Watts
Sea Clutter: Scattering, the K-Distribution and Radar Performance, 2nd ed. London: The Institute of Engineering Technology, 2013.

[25] B. Ristic, L. Rosenberg, D. Y. Kim, X. Wang, and J. Williams
A Bernoulli track-before-detect filter for maritime radar
IET Radar Sonar Navigation, vol. 14, no. 3, pp. 356–363, 2020.

[26] D. Y. Kim, B. Ristic, R. Guan, and L. Rosenberg
A Bernoulli track-before-detect filter for interacting targets in maritime radar
IEEE Trans. Aerosp. Electron. Syst., vol. 57, no. 3, pp. 1981–1991, Jun. 2021.

[27] A. Farina and S. Pardini
Track-while-scan algorithm in a clutter environment
IEEE Trans. Aerosp. Electron. Syst., no. 5, pp. 769–779, Sep. 1978.

[28] D. Y. Kim, B. Ristic, L. Rosenberg, R. Guan, and R. Evans
Exploiting Doppler in Bernoulli track-before-detect
in *Proc. IEEE Radar Conf.*, Atlanta, GA, USA, 2021.

[29] L. Rosenberg, S. Watts, and S. Bocquet
Scanning radar simulation in the maritime environment
in *Proc. IEEE Radar Conf.*, Florence, Italy, 2020.

[30] S. Watts
Modeling and simulation of coherent sea clutter
IEEE Trans. Aerosp. Electron. Syst., vol. 48, no. 4, pp. 3303–3317, 2012.

[31] S. Watts, L. Rosenberg, S. Bocquet, and M. Ritchie
Doppler spectra of medium grazing angle sea clutter; Part 2: Model assessment and simulation
IET Radar, Sonar Navigation, vol. 10, no. 1, pp. 32–42, 2016.

[32] K. J. Sangston and A. Farina
Coherent radar detection in compound-Gaussian clutter: Clairvoyant detectors
IEEE Aerosp. Electron. Syst. Mag., vol. 31, no. 11, pp. 42–63, Nov. 2016.

[33] A. Farina and P. Lombardo
Modelling of a mixture of k-distributed and gaussian clutter for coherent radar detection
Electron. Lett., vol. 30, no. 6, pp. 520–521, 1994.

[34] D. A. Abraham and A. P. Lyons
Novel physical interpretations of k-distributed reverberation
IEEE J. Ocean. Eng., vol. 27, no. 4, pp. 800–813, Oct. 2002.

[35] Y. Bar-Shalom, X. R. Li, and T. Kirubarajan
Estimation With Applications to Tracking and Navigation. New York, NY, USA: Wiley, 2001.

[36] J. Sun, C. Liu, Q. Li, and X. Chen
Labelled multi-Bernoulli filter with amplitude information for tracking marine weak targets
IET Radar, Sonar Navigation, vol. 13, no. 6, pp. 983–991, 2019.

[37] B. Ristic, D. Clark, B.-N. Vo, and B.-T. Vo
Adaptive target birth intensity for PHD and CPHD filters
IEEE Trans. Aerosp. Electron. Syst., vol. 48, no. 2, pp. 1656–1668, Apr. 2012.

[38] D. Schuhmacher, B.-T. Vo, and B.-N. Vo
A consistent metric for performance evaluation of multi-object filters
IEEE Trans. Signal Process., vol. 56, no. 8, pp. 3447–3457, Aug. 2008.